Electronic Supplementary Information

Highly Selective Adsorption of Ethylene over Ethane in a MOF Featuring the Combination of Open Metal Site and π-Complexation

Yiming Zhang,[a] Baiyan Li,[a,d,*] Rajamani Krishna,[b] Zili Wu,[c] Dingxuan Ma,[d] Zhan Shi,[d] Tony Pham,[a] Katherine Forrest,[a] Brian Space,[a] and Shengqian Ma[a,*]

[a]Department of Chemistry, University of South Florida, 4202 E. Fowler Avenue, Tampa, FL 33620, USA.

[b]Van't Hoff Institute for Molecular Sciences, University of Amsterdam, Science Park 904, 1098 XH Amsterdam, Netherlands.

[c]Center for Nanophase Materials Science and Chemical Science Division, Oak Ridge National Laboratory, TN 37831, USA.

[d]State Key Laboratory of Inorganic Synthesis and Preparative Chemistry, College of Chemistry, Jilin University, Changchun 130012, People's Republic of China.

E-mail: sqma@usf.edu; libaiyan@gmail.com

Experimental Details

All Starting materials, reagents, and solvents were purchased from commercial sources (Aldrich, Alfa, Fisher and Acros) and used without further purification.

Synthesis of MIL-101-Cr-SO_3H

MIL-101-Cr-SO_3H was synthesized according to the procedures reported the literature.[1]

Synthesis of MIL-101-Cr-SO_3Ag

To the 15 ml CH_3CN/H_2O (1:1) solution, 100 mg MIL-101-Cr-SO_3H and 100 mg $AgBF_4$ were added. The mixture was stirred under room temperature for 12 h, and then the solid was collected by filtration followed by washing with CH_3CN and water. The whole process was performed carefully under dark place. This exchanged process was conducted for three times, and then dried at 110 ºC for further test. ICP: Cr: 11%; Ag: 11.6%.

Characterization Details

PXRD data were collected on a Rigaku D/max 2550 Powder X-ray Diffractometer. N_2, C_2H_4, and C_2H_6 gas sorption isotherms were collected on a Micrometrics ASAP2020 Surface Area Analyzer. Elemental analyses were performed on a Perkin-Elmer 2400 element analyzer. XPS measurements were performed on an ESCALAB 250 X-ray photoelectron spectroscopy, using Mg Kα X-ray as the excitation source.

In situ IR experiments

IR spectra of ethylene adsorption were collected using a Thermo Nicolet Nexus 670 spectrometer in diffuse reflectance mode (DRIFTS). The MIL-101-Cr-SO_3Ag sample, ca. 5 mg, was treated in a DRIFTS cell (HC-900, Pike Technologies) at 423 K in helium (30 mL/min) for 1 hour to removal water and other adsorbates. The sample was then cooled down to room temperature for ethylene adsorption. The adsorption was conducted by flowing 10% ethylene/He (30 mL/min) over the sample for 5 min and then desorption was done in flowing helium. IR spectra were recorded continuously to follow the surface changes during the adsorption and desorption process. All reported IR spectra are difference spectra referenced to

a background spectrum collected at room temperature after pre-treatment but prior to ethylene adsorption.

Fitting of pure component isotherms

The measured experimental isotherm data for C_2H_4, and C_2H_6 on MIL-101-Cr-SO_3Ag were fitted with the dual-Langmuir-Freundlich isotherm model

$$q = q_{A,sat}\frac{b_A p^{\nu_A}}{1+b_A p^{\nu_A}} + q_{B,sat}\frac{b_B p^{\nu_B}}{1+b_B p^{\nu_B}} \qquad (1)$$

For fitting of the corresponding isotherms for C_2H_6 on MIL-101-Cr-SO_3Ag, a simpler 1-site Langmuir-Freundlich model was of adequate accuracy. The fit parameters for C_2H_4, and C_2H_6 are specified in Table S1. Fig. S7 presents a comparison of the experimentally determined component loadings for C_2H_4, and C_2H_6 on MIL-101-Cr-SO_3Ag at 296 K with the isotherm fits using parameters specified in Table 0. The fits are excellent over the entire range of pressures.

The pure component isotherm data for MIL-101-Cr, and MIL-101-Cr-SO_3H could be fitted with single site Langmuir-Freundlich model; the fit parameters are provided in Table S2, and Table S3, respectively.

Calculations of adsorption selectivity

The selectivity of preferential adsorption of C_2H_4 (component 1) over C_2H_6 (component 2) in a mixture containing 1 and 2, can be formally defined as

$$S_{ads} = \frac{q_1/q_2}{p_1/p_2} \qquad (2)$$

In equation (2), q_1 and q_2 are the component loadings of the adsorbed phase in the mixture. The calculations of S_{ads} are based on the use of the Ideal Adsorbed Solution Theory (IAST) of Myers and Prausnitz.[2]

Isosteric heats of adsorption

The isosteric heat of adsorption, Q_{st}, were calculated using the Clausius-Clapeyron equation by differentiation of the dual-Langmuir-Freundlich fits of the isotherms at two different temperatures, 296 K and 318 K with T-dependent parameters.

Simulations of C_2H_4/C_2H_6 breakthroughs in packed beds

In order to demonstrate the feasibility of producing 99.95%+ pure C_2H_4 in a Pressure Swing Adsorption (PSA) we carried out breakthrough simulations for C_2H_4/C_2H_6 mixtures in a fixed bed of length L, packed with MIL-101-Cr-SO_3Ag that has a framework density ρ = 700 kg/m^3; see schematic in Fig. S8. The voidage of the fixed bed was chosen $\varepsilon = 0.75$.

Assuming plug flow of the binary gas mixture through the fixed bed maintained under isothermal conditions at 296 K, the partial pressures in the gas phase at any position and instant of time are obtained by solving the following set of partial differential equations for each of the species i in the gas mixture.[3-9]

$$\frac{1}{RT}\frac{\partial p_i(t,z)}{\partial t} = -\frac{1}{RT}\frac{\partial\left(v(t,z)\,p_i(t,z)\right)}{\partial z} - \frac{(1-\varepsilon)}{\varepsilon}\rho\frac{\partial \bar{q}_i(t,z)}{\partial t}; \quad i = 1,2,...n \qquad (3)$$

In equation (3), t is the time, z is the distance along the adsorber, ρ is the framework density, ε is the bed voidage, v is the interstitial gas velocity, and $\bar{q}_i(t,z)$ is the *spatially averaged* molar loading within the crystallites of radius r_c, monitored at position z, and at time t. If the values of intra-crystalline diffusivities are large enough to ensure that

intra-crystalline gradients are absent and the entire crystallite particle can be considered to be in thermodynamic equilibrium with the surrounding bulk gas phase at that time *t*, and position *z* of the adsorber

$$\bar{q}_i(t,z) = q_i(t,z) \qquad (4)$$

The molar loadings q_i are calculated on the basis of adsorption equilibrium with the bulk gas phase partial pressures p_i at that position *z* and time *t*. The adsorption equilibrium can be calculated on the basis of the IAST. After discretization of the fixed bed into 100-200 slices, Equations (3) and Equation (4) need to be solved simultaneously using robust numerical procedures that are described in detail in the published literature.[10] The breakthrough simulation methodology has been rigorously tested and validated using a variety of experimental data on breakthroughs.[10]

The breakthrough characteristics for any component is essentially dictated by the characteristic contact time $\frac{L}{v} = \frac{L\varepsilon}{u}$ between the crystallites and the surrounding fluid phase. It is common to use the dimensionless time, $\tau = \frac{tu}{L\varepsilon}$, obtained by dividing the actual time, *t*, by the characteristic time, $\frac{L\varepsilon}{u}$ when plotting simulated breakthrough curves as has been done in Fig. S9.[10,11]

Let us first consider the adsorption phase of the PSA operations. Fig. S9 shows transient breakthrough of an equimolar C_2H_4/C_2H_6 mixture in an adsorber bed packed with MIL-101-Cr-SO_3Ag. The inlet gas is maintained at partial pressures $p_1 = p_2 = 50$ kPa. The more poorly adsorbed saturated alkane breaks through earlier and can be recovered in nearly pure form. From the gas phase concentrations at the exit of the adsorber, we can determine the % C_2H_6; this information is presented in Fig. S10. During the adsorption cycle, C_2H_6 at

purities > 99% can be reovered for a certain duration of the adsorption cycle indicated by the arrow in Fig. S10.

Once the entire bed is in equilibrium with the partial pressures $p_1 = p_2 = 50$ kPa, the desorption, "blowdown" cycle is initiated, by applying a vacuum or purging with inert gas. Fig. S11 shows $\%C_2H_4$ in the outlet gas of an adsorber bed packed with MIL-101-Cr-SO_3Ag in the desorption cycle. For production of ethylene as feedstock for polymerization purposes, the required purity level is 99.95%+ can be recovered during the time interval indicated by the arrow in Fig. S11.

Notation

b_A	dual-Langmuir-Freundlich constant for species *i* at adsorption site A, $Pa^{-\nu_i}$
b_B	dual-Langmuir-Freundlich constant for species *i* at adsorption site B, $Pa^{-\nu_i}$
c_i	molar concentration of species *i* in gas mixture, mol m^{-3}
c_{i0}	molar concentration of species *i* in gas mixture at inlet to adsorber, mol m^{-3}
L	length of packed bed adsorber, m
p_i	partial pressure of species *i* in mixture, Pa
p_t	total system pressure, Pa
q_i	component molar loading of species *i*, mol kg^{-1}
$q_{sat,A}$	saturation loading of site A, mol kg^{-1}
$q_{sat,B}$	saturation loading of site B, mol kg^{-1}
$\bar{q}_i(t)$	*spatially averaged* component molar loading of species *i*, mol kg^{-1}
R	gas constant, 8.314 J mol^{-1} K^{-1}
S_{ads}	adsorption selectivity, dimensionless
t	time, s
T	absolute temperature, K
u	superficial gas velocity in packed bed, m s^{-1}
v	interstitial gas velocity in packed bed, m s^{-1}
z	distance along the adsorber, and along membrane layer, m

Greek letters

ε	voidage of packed bed, dimensionless
ν	exponent in dual-Langmuir-Freundlich isotherm, dimensionless
ρ	framework density, kg m^{-3}
τ	time, dimensionless

Subscripts

i	referring to component *i*

A	referring to site A
B	referring to site B

Table S1. Dual-Langmuir-Freundlich fits for C_2H_4 and C_2H_6 at 296 K in MIL-101-Cr-SO_3Ag.

T-dependent fits for 296 K and 318 K isotherm data

$$b_A = b_{A0}\exp\left(\frac{E_A}{RT}\right); \quad b_B = b_{B0}\exp\left(\frac{E_B}{RT}\right)$$

	Site A				Site B			
	$q_{A,sat}$ mol kg^{-1}	b_{A0} Pa$^{-\nu_i}$	E_A kJ mol^{-1}	ν_A dimensionless	$q_{B,sat}$ mol kg^{-1}	b_{B0} Pa$^{-\nu_i}$	E_B kJ mol^{-1}	ν_B dimensionless
C_2H_4	2.3	6.22×10^{-6}	22	0.35	3.3	4.01×10^{-9}	6	1.46
C_2H_6	8.3	7.06×10^{-8}	13.6	0.84				

Table S2. Langmuir-Freundlich fits for C_2H_4 and C_2H_6 in MIL-101-Cr.

	$q_{A,sat}$ mol kg^{-1}	b_{A0} Pa$^{-\nu_i}$	E_A kJ mol^{-1}	ν_A dimensionless
C_2H_4	5.2	1.83×10^{-11}	35.4	0.95
C_2H_6	7.5	2.47×10^{-7}	10	0.9

Table S3. Langmuir-Freundlich fits for C_2H_4 and C_2H_6 in MIL-101-Cr-SO_3H.

	$q_{A,sat}$ mol kg^{-1}	b_{A0} Pa$^{-\nu_i}$	E_A kJ mol^{-1}	ν_A dimensionless
C_2H_4	6.7	1.31×10^{-6}	7.8	0.82
C_2H_6	6.3	1.2×10^{-7}	13	0.85

The investigation of interaction between ethylene and Ag+ or open metal sites.

Electronic structure calculations were performed to investigate the interaction between ethylene and Ag^+ ion. A $(C_6H_3(CO_2)_2)SO_3Ag$ cluster was considered for this calculation since it is expected that MIL-101-Cr-SO_3Ag contains this moiety. Starting with the sulfonyl terephthalate unit, a silver ion was placed in proximity to the oxygen atoms of the sulfonate group. The Ag^+ ion was optimized to an energetically favorable position within the cluster. The optimization was performed using density functional theory (DFT) with the well-known B3LYP functional. For this calculation, the 6-31G* basis set was used for all C, H, O, and S atoms, whereas the aug-cc-pVDZ-PP basis set[12] was used for Ag since a very large basis set was required to treat the inner electrons of this many-electron species. The optimized position for the Ag^+ ion was discovered to be 2.18 Å from one RSO_3^- oxygen atom and 2.19 Å from another oxygen atom.

Afterwards, an optimized ethylene molecule was placed in proximity to the Ag^+ ion in the $(C_6H_3(CO_2)_2)SO_3Ag$ cluster. The optimization of the C_2H_4–Ag^+ interaction was executed

using DFT using the same functional and basis sets for all atoms as described above. It was observed that the C_2H_4 molecule adsorbed closely to the Ag^+ ion in the cluster. The distances between the Ag^+ ion and the carbon atoms of the C_2H_4 molecule were found to be 2.18 and 2.19 Å. These distances are representative of a strong physisorption interaction. Note, the $C(C_2H_4)$–Ag^+ distances calculated in this work are notably shorter than the distances that were observed for the interaction between a silver ion and the unsaturated carbon atoms of a propylene molecule from previous work.[13]

A similar calculation was performed to examine the interaction between ethylene and an open-metal Cr^{3+} ion. A $[Cr_3O(O_2CH)_6]^+$ cluster, taken from the crystal structure of MIL-101-Cr, was used for this calculation. The SBKJC VDZ ECP[14] basis set was assigned to Cr for the calculations. This is a smaller basis set than what was used for Ag since Cr does not have as many electrons as Ag. A C_2H_4 molecule was placed in the vicinity of one of the Cr^{3+} ions and the molecule was relaxed using the same DFT methods as implemented above. The calculations revealed that the C_2H_4 molecule is further away from the Cr^{3+} ion as compared to the Ag^+ ion. Indeed, the optimized $C(C_2H_4)$–Cr^{3+} distances were observed to be 2.54 and 2.55 Å. This signifies a weaker interaction compared to the aforementioned $C(C_2H_4)$–Ag^+ distances. All calculations were performed using the NWChem software.[15]

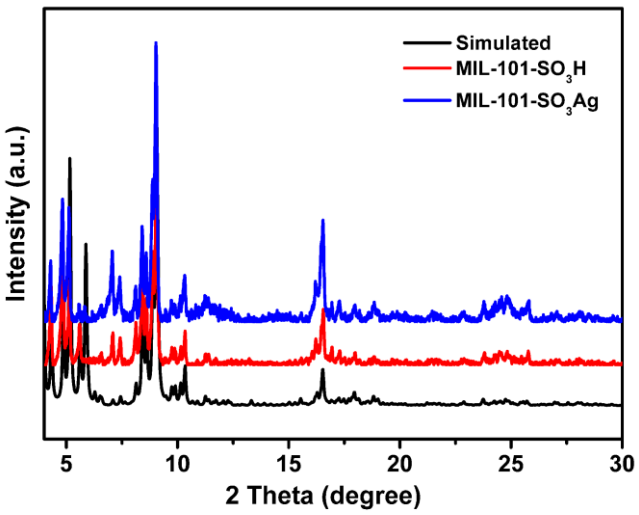

Fig. S1. Comparison of XRD of simulated MIL-101-Cr-SO_3H (black), MIL-101-Cr-SO_3H (red), and MIL-101-Cr-SO_3Ag (blue).

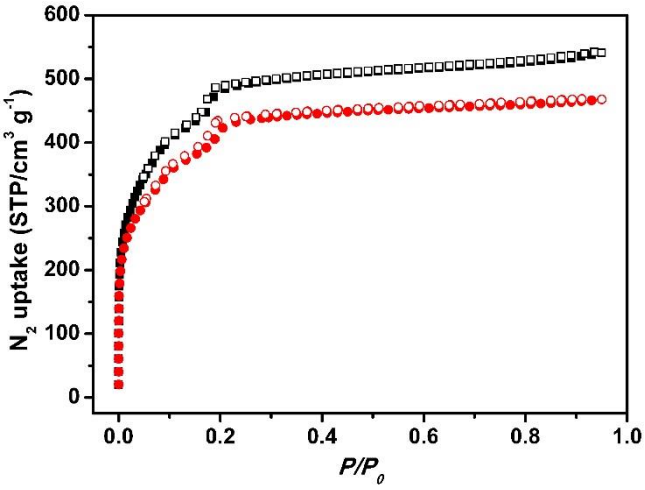

Fig. S2. Comparison of N_2 sorption MIL-101-Cr-SO_3H (black), MIL-101-Cr-SO_3Ag (red).

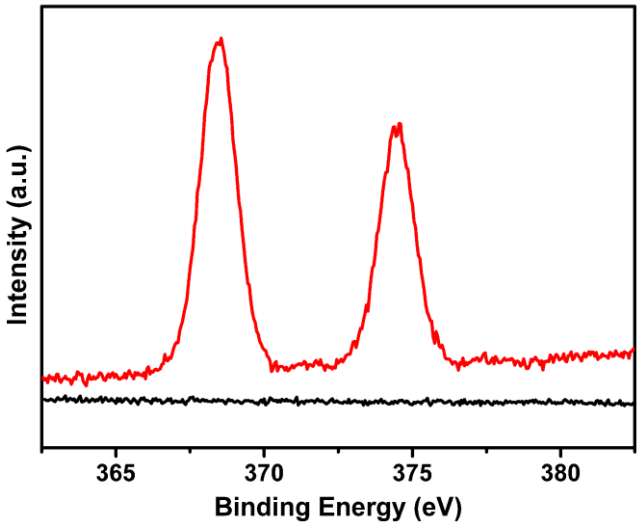

Fig. S3. Comparison of Ag(I) XPS of MIL-101-Cr-SO_3H (black) and MIL-101-Cr-SO_3Ag (red).

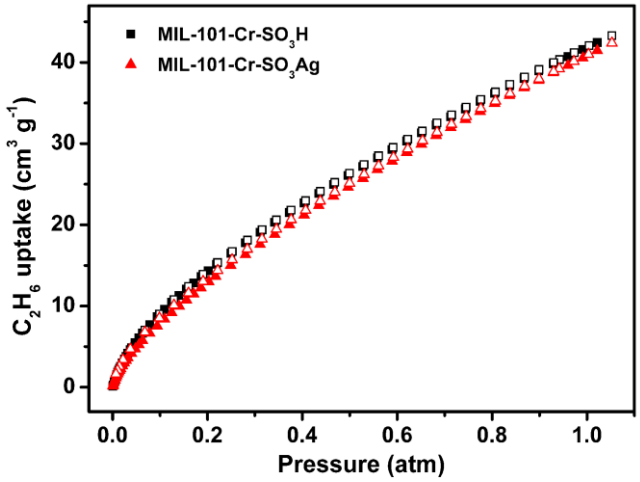

Fig. S4. Comparison of ethane sorption isotherms of MIL-101-Cr-SO_3H (black), and MIL-101-Cr-SO_3Ag (red) at 296 K.

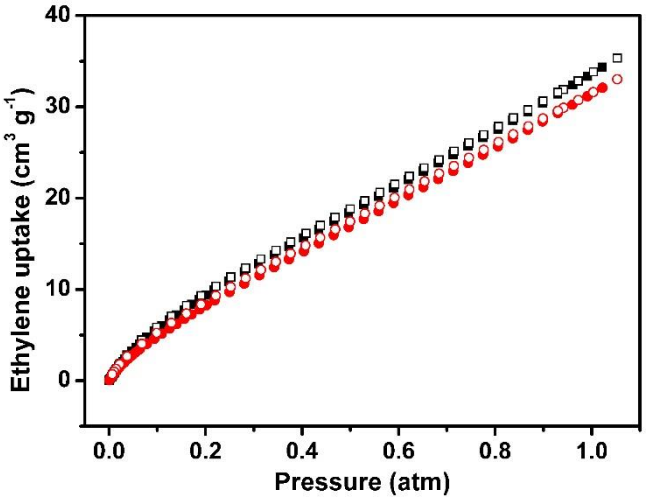

Fig. S5. Comparison of ethane sorption isotherms of MIL-101-Cr-SO_3H (black), and MIL-101-Cr-SO_3Ag (red) at 318 K.

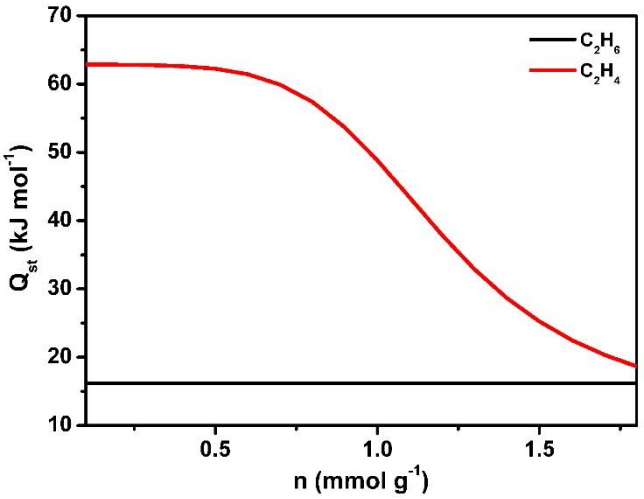

Fig. S6. Comparison of isosteric heats of adsorption for ethylene (red) and ethane (black) in MIL-101-Cr-SO_3Ag.

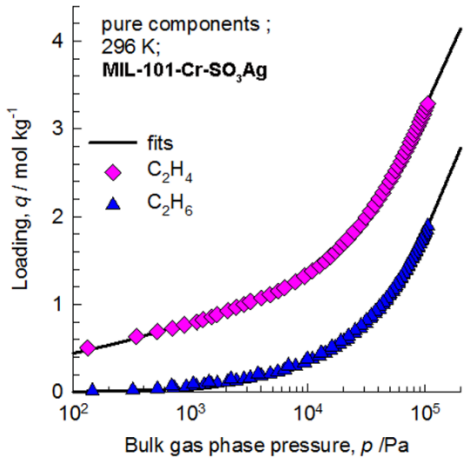

Fig. S7. Comparison of the experimentally determined component loadings for C_2H_4, and C_2H_6 on MIL-101-Cr-SO_3Ag at 296 K with the isotherm fits using parameters specified in Table S1.

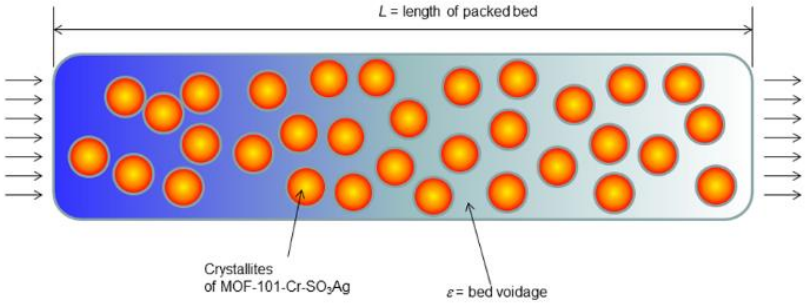

Fig. S8. Schematic of a packed bed adsorber. The parameter values used in the simulations presented here are: L = 0.12 m; voidage of bed, ε = 0.75; interstitital gas velocity, v= 0.003 m/s, superficial gas velocity, u = 0.00225 m/s.

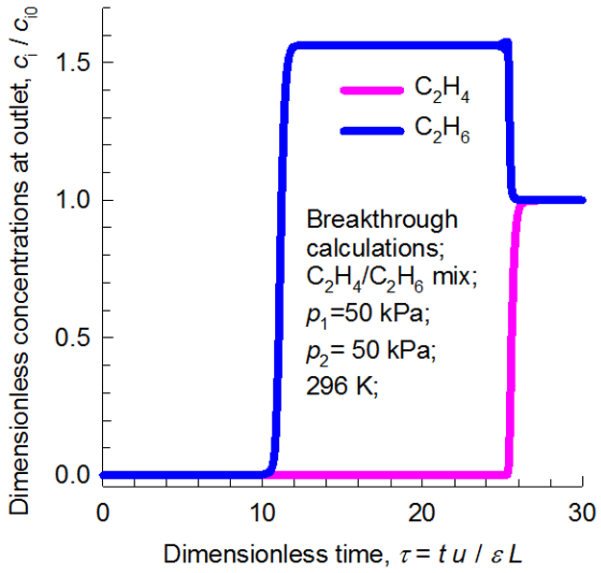

Fig. S9. Transient breakthrough of an equimolar C_2H_4/C_2H_6 mixture in an adsorber bed packed with MIL-101-Cr-SO_3Ag in the adsorption phase of a PSA operation. The inlet gas is maintained at partial pressures $p_1 = p_2 = 50$ kPa, at a temperature of 296 K.

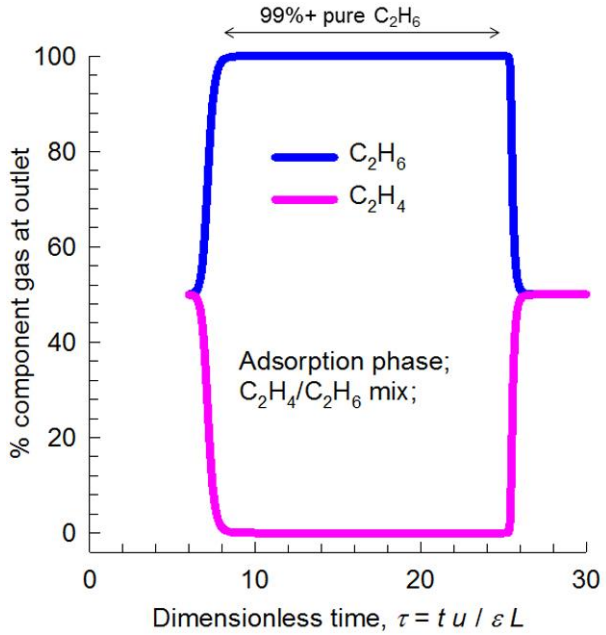

Fig. S10. % C_2H_6 in the outlet gas of an adsorber bed packed with MIL-101-Cr-SO_3Ag in the adsorption cycle. The inlet gas is maintained at partial pressures $p_1 = p_2 = 50$ kPa, at a temperature of 296 K.

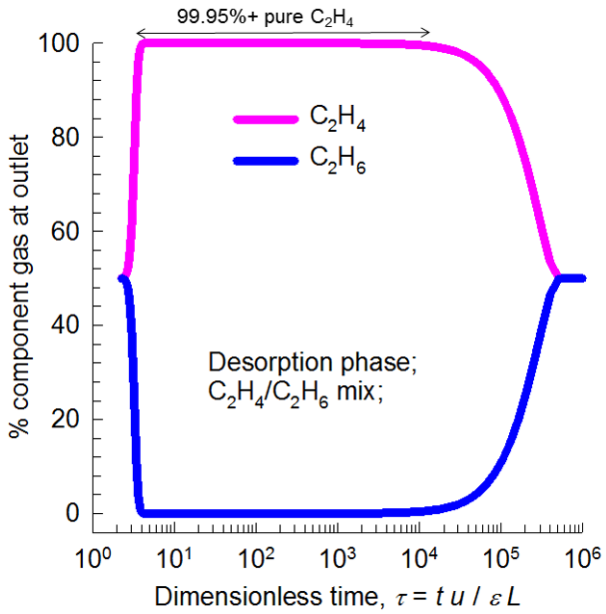

Fig. S11. % C_2H_4 in the outlet gas of an adsorber bed packed with MIL-101-Cr-SO_3Ag in the desorption cycle. The contents of the bed, that is equilibrated at partial pressures $p_1 = p_2 = 50$ kPa, at a temperature of 296 K is purged by inert gas. For the calculations presented in the graph, the inert gas is not included in the calculation of the % compositions.

Reference.

(1) G. Akiyama, R. Matsuda, H. Sato, M. Takata, and S. Kitagawa, *Adv. Mater.*, 2011, **23**, 3294.

(2) A. L. Myers, J. M. Prausnitz, *A.I.Ch.E.J.*, 1965, **11**, 121.

(3) D. M. Ruthven, Principles of Adsorption and Adsorption Processes, John Wiley: New York, 1984.

(4) D. M. Ruthven, S. Farooq, K. S. Knaebel, Pressure swing adsorption, VCH Publishers: New York, 1994.

(5) R. T. Yang, Gas separation by adsorption processes, Butterworth: Boston, 1987.

(6) D. D. Do, Adsorption analysis: Equilibria and kinetics, Imperial College Press: London, 1998.

(7) L. J. P. van den Broeke, R. Krishna, *Chem. Eng. Sci.*, 1995, **50**, 2507.

(8) K. S. Walton, M. D. LeVan, *Ind. Eng. Chem. Res.*, 2003, **42**, 6938.

(9) R. Krishna, R. Baur, *Sep. Purif. Technol.*, 2003, **33**, 213.

(10) R. Krishna, *Microporous Mesoporous Mater.*, 2014, **185**, 30.

(11) R. Krishna, J. R. Long, *J. Phys. Chem. C*, 2011, **115**, 12941.

(12) K. A. Peterson, C. Puzzarini, *Theor. Chem. Acc.*, 2005, **114**, 283.

(13) K. C. Kim, C. Y. Lee, D. Fairen-Jimenez, S. T. Nguyen, J. T. Hupp, R. Q. Snurr, *J. Phys. Chem. C*, 2014, **118**, 9086.

(14) (a) W. J. Stevens, M. Krauss, H. Basch, P. G. Jasien, *Can. J. Chem.*, 1992, **70**, 612; (b) T. R. Cundari, W. J. Stevens, *J. Chem. Phys.*, 1993, **98**, 5555.

(15) M. Valiev, E. Bylaska, N. Govind, K. Kowalski, T. Straatsma, H. V. Dam, D. Wang, J. Nieplocha, E. Apra, T. Windus, W. de Jong, *Comput. Phys. Commun.*, 2010, **181**, 1477.